Gradient of image-space wave-equation tomography in the generalized source domain by the adjoint-state method

Claudio Guerra

(September 24, 2009)

Running head: **Gradient of ISWET by the adjoint-state method**

ABSTRACT

Optimization using gradient descent techniques requires the computation of the gradient of the objective function. The adjoint-state method is an efficient way of computing the gradient, since is not necessary to compute the expensive Frechét derivatives. Here, I derive the gradient of the image-space wave-equation tomography using the adjoint-state method and show its application with a numerical example.

INTRODUCTION

Wave-equation tomography aims to solve for Earth models that explain the data under some norm. Two main categories exist depending on the domain the objective function is computed. In one category, known as waveform inversion (Lines and Treitel, 1984; Tarantola, 1987; Woodward, 1992), the objective function is defined in the data space where the modeled data are compared with the recorded seismograms. In the other category, ~~generally~~ called here image-space wave-equation tomography (ISWET), the minimization of the objective function is performed in the image space. Wave-equation migration velocity analysis (WEMVA) (Sava and Biondi, 2004a,b) and differential semblance velocity analysis (DSVA) (Shen, 2004; Shen and Symes, 2008) are two variants of ISWET.

Despite their differences, those two categories are linked by the concept of extended modeling (Symes, 2008). Symes (2008) showed that ISWET can be regarded as a solution method for the partially linearized waveform inversion. While ISWET solves for the long-wavelength components of the slowness model, assuring global convergence, waveform inversion computes the short-wavelength components, ~~providing~~ accuracy.

~~Similar to~~ waveform inversion, ISWET is a computationally demanding process. Generalized sources are commonly used to decrease this computational cost (Shen and Symes, 2008; Tang et al., 2008). Because wavefield propagation is a linear process, generalized sources are computed by linearly combining source wavefields and receiver wavefields, using phase-encoding techniques (Whitmore, 1995; Romero et al., 2000). In particular, Guerra et al. (2009) used generalized source functions synthesized by phase-encoding modeling experiments in the image space to drastically decrease the cost of DSVA. The numerical example showed in this report also uses this kind of generalized source ~~functions.~~

The aforementioned ISWET methods seek ~~for~~ the optimal slowness by driving an image perturbation to a minimum. However, they differ ~~on~~ the way the image perturbation is computed and, consequently, ~~on~~ the numerical optimization scheme applied. As Biondi (2008) points out, WEMVA is not easily automated. The image perturbation is computed by the linearized residual prestack depth migration (Sava and Biondi, 2004a), ~~that~~ uses a manually picked residual-moveout parameter. However, as the perturbed image is consistent with the wave-equation tomographic operator, conjugate-gradient methods can be used to invert for the slowness perturbation. In DSVA, the perturbed image is computed by applying the fully automated differential-semblance operator (DSO) to the subsurface-offset gathers (ODCIG) or angle gathers (ADCIG). When applied to ODCIG, DSVA minimizes the energy not focused at zero-offset. When applied to ADCIG, DSVA minimizes energy departing from flatness of the reflectors. Notwithstanding the ability of automating ISWET, DSVA produces perturbed images not consistent with the wave-equation tomographic operator. To minimize the objective function computed with DSO, quasi-Newton algorithms are used for which the gradient of the objective function needs to be computed.

The gradient of the objective function can be obtained by computing the Frechét derivatives. However, this computation even for 2D applications of ISWET can be very expensive. The adjoint-state method (Chavent and Jacewitz, 1995; Plessix, 2006) is an efficient way to compute the gradient without using Frechét derivatives. Plessix (2006) describes two methodologies for computing the gradient of the objective function using the adjoint-state method. The more intuitive uses the augmented Lagrangian. The augmented Lagrangian is formed by the objective function and the scalar product of the adjoint-state variables ~~and~~ general solutions of the forward modeling equations. The adjoint-state variables, in turn, are solution of a system of adjoint-state equations defined by equating to zero the derivative

of the augmented Lagrangian with respect to the state variables. For the linear case, the adjoint of the modeling operator applied to the adjoint-state variables gives the gradient of the objective function.

Here, I derive the gradient of the ISWET objective function using the augmented Lagrangian methodology. The reasoning presented here is valid whether ISWET uses areal-shot migration or shot-profile migration. Tang et al. (2008) provide a complete description of the forward and adjoint wave-equation tomographic operators in the generalized source domain. ~~The goal of this paper is to provide a more detailed~~ derivation of the gradient of the ISWET objective function using the adjoint-state method ~~than the ones available,~~ for example, Shen et al. ~~(~~2003~~)~~.

~~The references on~~ the image-space phase-encoded gathers ~~are~~ Biondi (2006, 2007) and Guerra and Biondi (2008a). For completeness, here I briefly describe how to compute these phase-encoded gathers. Then~~,~~ I derive the ISWET gradient using the adjoint-state method and~~, finally~~ show an example of DSVA using image-space phase-encoded gathers on the Marmousi model.

IMAGE-SPACE GENERALIZED SOURCES

Biondi (2006, 2007) introduced the concept of prestack exploding-reflector as a generalization of the exploding-reflector ~~modeling~~ (**?**). ~~It~~ synthesizes areal data and the corresponding areal source function, having as initial condition a prestack image computed with wave-equation migration. If the slowness is accurate and the energy is focused at zero-subsurface offset, it reduces to the conventional exploding-reflector ~~modeling. Basically,~~ prestack exploding-reflector models one single reflection event from one single ODCIG by

~~the~~ recursive upward continuation with the following one-way wave equations:

$$\begin{cases} \left(\frac{\partial}{\partial z} - i\sqrt{\omega^2 \hat{s}^2(\mathbf{x}) - |\mathbf{k}|^2}\right) d(\mathbf{x}, \omega; x_m, y_m) = r_D(\mathbf{x}, \mathbf{h}; x_m, y_m) \\ d(x, y, z = z_{\max}, \omega; x_m, y_m) = 0 \end{cases}, \tag{1}$$

and

$$\begin{cases} \left(\frac{\partial}{\partial z} + i\sqrt{\omega^2 \hat{s}^2(\mathbf{x}) - |\mathbf{k}|^2}\right) u(\mathbf{x}, \omega; x_m, y_m) = r_U(\mathbf{x}, \mathbf{h}; x_m, y_m) \\ u(x, y, z = z_{\max}, \omega; x_m, y_m) = 0 \end{cases}, \tag{2}$$

where $r_D(\mathbf{x}, \mathbf{h}; x_m, y_m)$ and $r_U(\mathbf{x}, \mathbf{h}; x_m, y_m)$ are the isolated SODCIGs at the horizontal location (x_m, y_m) for a single reflector, and are suitable for the initial conditions for the source and receiver wavefields, respectively. They are obtained by rotating the original unfocused SODCIGs according to the apparent geological dip of the reflector. This rotation maintains the velocity information needed for migration velocity analysis, especially for dipping reflectors (Biondi, 2007). $d(x, y, z = z_c, \omega; x_m, y_m)$ is the areal source data and $u(x, y, z = z_c, \omega; x_m, y_m)$ is the areal receiver data for a single reflector and a single SODCIG located at (x_m, y_m); $z = z_c$ denotes that the wavefields can be collected at any depth level, z_c. This characteristic is important to accelerate ISWET, especially if z_c separates regions of sufficiently accurate slowness above and inaccurate slowness below. As a consequence, the synthesized gathers are naturally 'datumized' and the wavefield propagations during ISWET can be restricted to the region where the slowness model must be updated. This feature allows ISWET to be applied in a target-oriented manner.

As initially formulated, however, if one ~~considers to model one~~ single reflection from one ~~single~~ SODCIG at a time, the prestack exploding-reflector ~~modeling~~ generates dataset that can be orders of magnitude bigger than the original dataset. As discussed by Biondi (2006); Guerra and Biondi (2008b,a), ~~by~~ modeling several reflectors and several SODCIGs simultaneously using random phase encoding a much smaller dataset ~~is obtained~~. The

randomly encoded areal source and areal receiver wavefields can be computed as follows:

$$\begin{cases} \left(\frac{\partial}{\partial z} - i\sqrt{\omega^2 \hat{s}^2(\mathbf{x}) - |\mathbf{k}|^2}\right) \widetilde{d}(\mathbf{x}, \mathbf{p}_m, \omega) = \widetilde{r}_D(\mathbf{x}, \mathbf{h}, \mathbf{p}_m, \omega) \\ \widetilde{d}(x, y, z = z_{\max}, \mathbf{p}_m, \omega) = 0 \end{cases}, \tag{3}$$

and

$$\begin{cases} \left(\frac{\partial}{\partial z} + i\sqrt{\omega^2 \hat{s}^2(\mathbf{x}) - |\mathbf{k}|^2}\right) \widetilde{u}(\mathbf{x}, \mathbf{p}_m, \omega) = \widetilde{r}_U(\mathbf{x}, \mathbf{h}, \mathbf{p}_m, \omega) \\ \widetilde{u}(x, y, z = z_{\max}, \mathbf{p}_m, \omega) = 0 \end{cases}, \tag{4}$$

where $\widetilde{r}_D(\mathbf{x}, \mathbf{h}, \mathbf{p}_m, \omega)$ and $\widetilde{r}_U(\mathbf{x}, \mathbf{h}, \mathbf{p}_m, \omega)$ are the encoded SODCIGs after rotations. They are defined as follows:

$$\widetilde{r}_D(\mathbf{x}, \mathbf{h}, \mathbf{p}_m, \omega) = \sum_{x_m} \sum_{y_m} r_D(\mathbf{x}, \mathbf{h}, x_m, y_m) \beta(\mathbf{x}, x_m, y_m, \mathbf{p}_m, \omega), \tag{5}$$

$$\widetilde{r}_U(\mathbf{x}, \mathbf{h}, \mathbf{p}_m, \omega) = \sum_{x_m} \sum_{y_m} r_U(\mathbf{x}, \mathbf{h}, x_m, y_m) \beta(\mathbf{x}, x_m, y_m, \mathbf{p}_m, \omega), \tag{6}$$

where $\beta(\mathbf{x}, x_m, y_m, \mathbf{p}_m, \omega) = e^{i\gamma(\mathbf{x}, x_m, y_m, \mathbf{p}_m, \omega)}$ is a pseudo-random phase-encoding function, with $\gamma(\mathbf{x}, x_m, y_m, \mathbf{p}_m, \omega)$ being a uniformly distributed random sequence in $\mathbf{x}$, x_m, y_m and ω; the variable $\mathbf{p}_m$ is the index of different realizations of the random sequence. The recursive solution of equations 3 and 4 gives the encoded areal source data $\widetilde{d}(x, y, z = z_c, \mathbf{p}_m, \omega)$ and areal receiver data $\widetilde{u}(x, y, z = z_c, \mathbf{p}_m, \omega)$, at the depth level, z_c.

GRADIENT COMPUTATION OF ISWET BY THE ADJOINT-STATE METHOD

Image-space wave-equation tomography aims to iteratively solve for the slowness model, $s = s(\mathbf{x})$, that minimizes the linearized objective function

$$J(s) = \frac{1}{2} ||\Delta r(s)||^2 = \frac{1}{2} ||r(s) - \mathbf{M} r(s)||^2, \tag{7}$$

where $\Delta r = \Delta r(\mathbf{x}, \mathbf{h})$ is the image perturbation that measures the ~~goodness~~ of the slowness model. Notice that the objective function depends on the slowness model through the image

perturbation. To computed Δr a differential residual-focusing operator, $\mathbf{M}$, is applied to the image, $r = r(\mathbf{x}, \mathbf{h})$, obtained with the current slowness (Biondi, 2008), using either differential residual prestack migration (Sava and Biondi, 2004a,b) or differential-semblance optimization (DSO) (Shen and Symes, 2008) operators. Herein, operators are represented by bold capital letters.

If the differential residual-focusing operator $\mathbf{M}$ is independent on the slowness, the gradient of this objective function evaluated at the current slowness, $\widehat{s} = \widehat{s}(\mathbf{x})$, is

$$\nabla J(s) = \left(\frac{\partial r}{\partial s}\right)' \Big|_{s=\widehat{s}} \left(\mathbf{I} - \mathbf{M}'\right) \Delta \widehat{r}. \tag{8}$$

where $'$ denotes the adjoint, $\mathbf{I}$ is the identity operator and $\Delta \widehat{r} = \Delta \widehat{r}(\mathbf{x}, \mathbf{h})$ is the perturbed image obtained with the current slowness model. The linear operator $\frac{\partial \widehat{r}}{\partial s}$ defines the mapping, $\frac{\partial \widehat{r}}{\partial s} \Delta s = \Delta r$, between the slowness perturbation Δs and the image perturbation and it is called image-space wave-equation tomographic operator.

As the image-space wave-equation tomographic operator is composed of different operators, it is difficult from equation 8 to envision which operations are performed to compute the gradient. Therefore, for a clear explanation of the operators involved, I use the adjoint-state method to derive the gradient of the objective function (equation 7).

In migration with generalized sources or shot-profile migration, the source and receiver wavefields are propagated independently and the image, $r_z = r_z(\mathbf{x}, \mathbf{h})$, at a depth level z, is computed by the crosscorrelation

$$r_z(\mathbf{x}, \mathbf{h}) = \sum_{\omega} d_z^*(\mathbf{x} - \mathbf{h}, \omega) u_z(\mathbf{x} + \mathbf{h}, \omega), \tag{9}$$

where $d_z(\mathbf{x}, \omega)$ is the source wavefield for a single frequency ω at horizontal coordinates $\mathbf{x} = (x, y)$; $u_z(\mathbf{x}, \omega)$ is the receiver wavefield and $\mathbf{h} = (h_x, h_y)$ is the subsurface half-offset,

and '*' stands for the complex-conjugate. An additional summation over shots is required when migrating more than one shot. Hereafter, letters d and u stand for source and receiver wavefields, respectively, irrespective to the migration scheme.

In a more compact notation, not explicitly writing the dependencies on $\mathbf{x}$ and $\mathbf{h}$, equation 9 can be written as:

$$r_z = \mathbf{S}\mathbf{D}'_z(\omega)u_z(\omega) = \mathbf{S}\mathbf{U}_z(\omega)d^*_z(\omega), \tag{10}$$

where $\mathbf{D}$ and $\mathbf{U}$ are convolutional operators composed of (h_x, h_y)-shifted versions of $d_z(\mathbf{x}, \omega)$ and $u_z(\mathbf{x}, \omega)$, respectively. Operator $\mathbf{S}$ corresponds to the summation over frequency.

For subsequent depth levels, $d(\mathbf{x}, \omega)$ is computed by means of the recursive downward propagation

$$\begin{cases} d_{z+1}(\omega) = \mathbf{T}^{\downarrow}_z(\omega, s)d_z(\omega) \\ d_1(\omega) = q(\omega), \end{cases} \tag{11}$$

where $\mathbf{T}^{\downarrow}_z$ is the downward continuation operator, which is function of the slowness, s, and $q(\omega)$ is the source wavefield used as boundary condition. In the case of conventional shot-profile migration, $q(\omega) = f_s(\omega)\delta(\mathbf{x} - \mathbf{x_s})$ is the source signature located at $\mathbf{x}_s = (x_s, y_s, 0)$. If using the generalized sources in the image space, $q(\omega)$ represents the image-space phase-encoded source wavefield of equation 3.

The downward continuation of the receiver wavefield is performed by

$$\begin{cases} u_{z+1}(\omega) = \mathbf{T}^{\downarrow}_z(\omega, s)u_z(\omega) \\ u_1(\omega) = w(\omega), \end{cases} \tag{12}$$

where $w(\omega)$ is the recorded data at the surface for shot-profile migration. If using generalized sources in the image space, $w(\omega)$ is the phase-encoded areal receiver wavefield of equation 4.

In equations 11 and 12, I omitted the dependencies of the wavefield with respect to $\mathbf{x}$. The subscript 1 in equations 11 and 12 represents the surface for the shot-profile migration and the 'collection' level, z_c, for the image-space phase-encoded wavefields.

In the image-space wave-equation tomography problem, the perturbed source and receiver wavefields and image perturbations are used to compute the slowness perturbation to update the current slowness model. From the perturbation theory, we have that $d = \widehat{d} + \Delta d$, $u = \widehat{u} + \Delta u$ and, consequently, $r = \widehat{r} + \Delta r$ are physical realizations with $s = \widehat{s} + \Delta s$, where the *hat* refers to fields obtained with the background slowness. To the first order (Born approximation), these perturbed fields are given by

$$\Delta d_{z+1}(\omega) = \mathbf{T}_z^{\downarrow}(\omega, \widehat{s}) \Delta d_z(\omega) + \widetilde{\widetilde{\mathbf{D}}}_z(\omega) \Delta s_z \tag{13}$$

$$\Delta u_{z+1}(\omega) = \mathbf{T}_z^{\downarrow}(\omega, \widehat{s}) \Delta u_z(\omega) + \widetilde{\widetilde{\mathbf{U}}}_z(\omega) \Delta s_z \tag{14}$$

The diagonal operators $\widetilde{\widetilde{\mathbf{D}}}_z$ and $\widetilde{\widetilde{\mathbf{U}}}_z$ have in the diagonal entries the scattered source and receiver wavefields, respectively. These wavefields are given by the action of the scattering operator $\Delta \mathbf{T}_z^{\downarrow}$ on the background wavefields

$$\widetilde{\widetilde{\mathbf{D}}}_z(\omega) = \Delta \mathbf{T}_z^{\downarrow}(\omega, \widehat{s}) \widehat{d}_z(\omega) = i \frac{\omega^2 \widehat{s}}{\sqrt{\omega^2 \widehat{s}^2 - |\mathbf{k}|^2}} dz \; \widehat{d}_z(\omega), \tag{15}$$

and

$$\widetilde{\widetilde{\mathbf{U}}}_z(\omega) = \Delta \mathbf{T}_z^{\downarrow}(\omega, \widehat{s}) \widehat{u}_z(\omega) = -i \frac{\omega^2 \widehat{s}}{\sqrt{\omega^2 \widehat{s}^2 - |\mathbf{k}|^2}} dz \; \widehat{u}_z(\omega). \tag{16}$$

The perturbed image is given by

$$\Delta r_z = \mathbf{S} \left(\widehat{\mathbf{U}}_z(\omega) \Delta d_z^*(\omega) + \widehat{\mathbf{D}}'_z(\omega) \Delta u_z(\omega) \right). \tag{17}$$

The matrix representation of equations 13, 14, 17 is

$$\Delta \underline{\mathbf{d}} = \mathbf{T}^{\downarrow} \Delta \underline{\mathbf{d}} + \widetilde{\widetilde{\mathbf{P}}} \mathbf{S}' \Delta \mathbf{s}, \tag{18}$$

$$\Delta\underline{\mathbf{u}} = \mathbf{T}^{\downarrow}\Delta\underline{\mathbf{u}} + \widetilde{\widetilde{\mathbf{U}}}\mathbf{S}'\Delta\mathbf{s}, \tag{19}$$

$$\Delta\underline{\mathbf{r}} = \mathbf{S}\left(\widehat{\mathbf{U}}\Delta\underline{\mathbf{d}}^{*} + \widehat{\mathbf{D}}'\Delta\underline{\mathbf{u}}\right), \tag{20}$$

where $\mathbf{S}'$ is a spreading operator that replicates the slowness perturbation for every frequency.

Equations 18, 19 and 20 are the forward modeling equations of the image-space wave-equation tomography problem using the generalized sources or shot-profile schemes. They depend on the state variables $\Delta\underline{\mathbf{d}}$, $\Delta\underline{\mathbf{u}}$ and $\Delta\underline{\mathbf{r}}$. Plessix (2006) describes how to compute the adjoint-states using the augmented functional methodology. By introducing the adjoint-state variables $\underline{\lambda}_d$, $\underline{\lambda}_u$ and $\underline{\lambda}_r$, the augmented Lagrangian reads

$$\begin{aligned}\mathcal{L}(\Delta\underline{\mathbf{d}}, \Delta\underline{\mathbf{u}}, \Delta\underline{\mathbf{r}}, \underline{\lambda}_d, \underline{\lambda}_u, \underline{\lambda}_r; \Delta\mathbf{s}) = \mathcal{R}\Big[&\tfrac{1}{2}\,||\Delta\underline{\mathbf{r}}||^2 - \\ &\left\langle \underline{\lambda}_d, \left(\mathbf{I} - \mathbf{T}^{\downarrow}\right)\Delta\underline{\mathbf{d}} - \widetilde{\widetilde{\mathbf{D}}}\mathbf{S}'\Delta\mathbf{s}\right\rangle - \\ &\left\langle \underline{\lambda}_u, \left(\mathbf{I} - \mathbf{T}^{\downarrow}\right)\Delta\underline{\mathbf{u}} - \widetilde{\widetilde{\mathbf{U}}}\mathbf{S}'\Delta\mathbf{s}\right\rangle - \\ &\left\langle \underline{\lambda}_r, \Delta\underline{\mathbf{r}} - \mathbf{S}\left(\widehat{\mathbf{U}}\Delta\underline{\mathbf{d}}^{*} + \widehat{\mathbf{D}}'\Delta\underline{\mathbf{u}}\right)\right\rangle\Big]\end{aligned}$$

The adjoint-state variables are computed by taking the derivative of $\mathcal{L}$ with respect to the state variables and equating to zero, which gives

$$\left(\mathbf{I} - \mathbf{T}^{\downarrow}\right)' \underline{\lambda}_d = \widehat{\mathbf{U}}\underline{\lambda}_r, \tag{21a}$$

$$\left(\mathbf{I} - \mathbf{T}^{\downarrow}\right)' \underline{\lambda}_u = \widehat{\mathbf{D}}\underline{\lambda}_r, \tag{21b}$$

$$\underline{\lambda}_r = \Delta\underline{\mathbf{r}}. \tag{21c}$$

Notice that

$$\left(\mathbf{I} - \mathbf{T}^{\downarrow}\right)' = \left(\mathbf{I} - \mathbf{T}^{\downarrow'}\right) = \left(\mathbf{I} - \mathbf{T}^{\uparrow}\right) \tag{22}$$

corresponds to the recursive upward propagation operator. Therefore, equations 21a and 21b can be written as

$$\underline{\lambda}_p = \mathbf{T}^{\uparrow}\underline{\lambda}_d + \widehat{\mathbf{U}}\underline{\lambda}_r, \tag{23a}$$

$$\underline{\lambda}_u = \mathbf{T}^{\uparrow}\underline{\lambda}_u + \widehat{\mathbf{D}}\underline{\lambda}_r, \tag{23b}$$

which correspond to the recursive upward propagation of the perturbed wavefields resulting from the convolution of the wavefields computed with the current slowness and the perturbed image.

The gradient of J is

$$\nabla_s J(\mathbf{s}) = \mathbf{S}\left(\widetilde{\widetilde{\mathbf{D}}}'\,\underline{\lambda}_d + \widetilde{\widetilde{\mathbf{U}}}'\,\underline{\lambda}_u\right). \tag{24}$$

To compute the gradient, the adjoint-state wavefields, $\underline{\lambda}_d$ and $\underline{\lambda}_u$, are upward propagated and cross-correlated in time with the scattered wavefields.

EXAMPLE

The gradient of the ISWET objective function computed in the previous section can be used in a quasi-Newton optimization scheme. I use L-BFGS-B bound constrained optimization algorithm (Nocedal and Wright, 2000) to invert for slowness using the Marmousi model. A B-spline smoothing, with nodes spaced at 240 m in x and 16 m in z, is applied to the gradient to prevent problems caused by poor illumination and noise. 375 two-way shots with 24 m spacing ~~were modeled~~ using the original Marmousi model of Figure 1a. The maximum offset is 6600 m.

Figure 1b shows the one-way shot profile image with the correct slowness model. The modeled data were also migrated using the background slowness of Figure 2a to compute the

background image of Figure 2b. The background slowness differs from the true slowness in a limited region as can be seen in Figure 3, which shows the ratio between true and background slowness. When comparing the two images, ~~it is clear the~~ pull-up effect caused by migrating with a too slow velocity at the center-bottom of the background image.

Following Guerra et al. (2009), representative reflectors were selected from the background image (Figure 4) to synthesize eleven image-space phase-encoded source and receiver wavefields using the background slowness. Prior to modeling, the selected reflectors were subjected to rotation according to the apparent geological dip as mentioned before.

Figure 5a shows the optimized slowness model after 4 iterations comprising 41 function and gradient evaluations. The optimized slowness decreased as expected, ~~however without recovering~~ the details of the true slowness. The smoothness of the optimized slowness ~~can be partially credited to~~ the B-spline filtering of the gradient and also because image-space wave-equation tomography ~~is not able to~~ solve for the short wavelengths of the slowness model, as ~~pointed out~~ by Symes (2008).

Figure 5b shows the shot-profile migration of the original shots using the optimized slowness. Notice that the pull-up effect ~~was~~ greatly mitigated and the reflectors are more focused than in the background image.

Figure 6 shows~~, from top to bottom,~~ the ADCIGs resulting from shot-profile migration of the original shots using the true slowness, the background slowness and the optimized slowness. The reflectors computed with the optimized slowness are flatter than that with the background slowness, ~~attesting~~ the higher accuracy of the optimized slowness.

CONCLUSION

I used the straightforward augmented Lagrangian methodology to derive the adjoint-state of the gradient of the objective function for the image-space wave-equation tomography problem. The derivation is valid whether one considers migration of shot-profiles or generalized sources. Image-space phase-encoded gathers were used to optimize the Marmousi slowness model, which significantly accelerates image-space wave-equation tomography. The quasi-Newton optimization ~~was able to increase~~ the accuracy of the slowness as the numerical example shows.

REFERENCES

Biondi, B., 2006, Prestack exploding-reflectors modeling for migration velocity analysis: 76th Ann. Internat. Mtg., Expanded Abstracts, 3056–3060, Soc. of Expl. Geophys.

———, 2007, Prestack modeling of image events for migration velocity analysis: **SEP-131**, 101–118.

———, 2008, Automatic wave-equation migration velocity analysis: **SEP-134**, 65–78.

Chavent, G. and C. A. Jacewitz, 1995, Determination of background velocities by multiple migration fitting: Geophysics, **60**, 476–490.

Guerra, C. and B. Biondi, 2008a, Phase-encoding with Gold codes for wave-equation migration: **SEP-136**.

———, 2008b, Prestack exploding reflector modeling: The crosstalk problem: **SEP-134**, 79–92.

Guerra, C., Y. Tang, and B. Biondi, 2009, Wave-equation tomography using image-space phase-encoded data: **SEP-138**, 95–116.

Lines, L. and S. Treitel, 1984, A review of least-squares inversion and its application to geophysical problems: Geophys. Prospecting, **32**, 159–186.

Nocedal, J. and S. Wright, 2000, Numerical optimization: Springer Verlag,New York.

Plessix, R.-E., 2006, A review of the adjoint-state method for computing the gradient of a functional with geophysical applications: Geophys. J. Int., **167**, 495–503.

Romero, L. A., D. C. Ghiglia, C. C. Ober, and S. A. Morton, 2000, Phase encoding of shot records in prestack migration: Geophysics, **65**, 426–436.

Sava, P. and B. Biondi, 2004a, Wave-equation migration velocity analysis-I: Theory: Geophysical Prospecting, **52**, 593–606.

———, 2004b, Wave-equation migration velocity analysis-II: Examples: Geophysical

Prospecting, **52**, 607–623.

Shen, P., 2004, Wave-equation Migration Velocity Analysis by Differential Semblance Optimization: PhD thesis, Rice University.

Shen, P. and W. W. Symes, 2008, Automatic velocity analysis via shot profile migration: Geophysics, **73**, VE49–VE59.

Shen, P., W. W. Symes, and C. C. Stolk, 2003, Differential semblance velocity analysis by wave-equation migration: SEG Technical Program Expanded Abstracts, **22**, 2132–2135.

Symes, B., 2008, Migration velocity analysis and waveform inversion: Geophysical Prospecting, **56**, 765–790.

Tang, Y., C. Guerra, and B. Biondi, 2008, Image-space wave-equation tomography in the generalized source domain: **SEP-136**, 1–22.

Tarantola, A., 1987, Inverse problem theory: Methods for data fitting and model parameter estimation: Elsevier.

Whitmore, N. D., 1995, An Imaging Hierarchy for Common Angle Plane Wave Seismogram: PhD thesis, University of Tulsa.

Woodward, M. J., 1992, Wave-equation tomography: Geophysics, **57**, 15–26.

LIST OF FIGURES

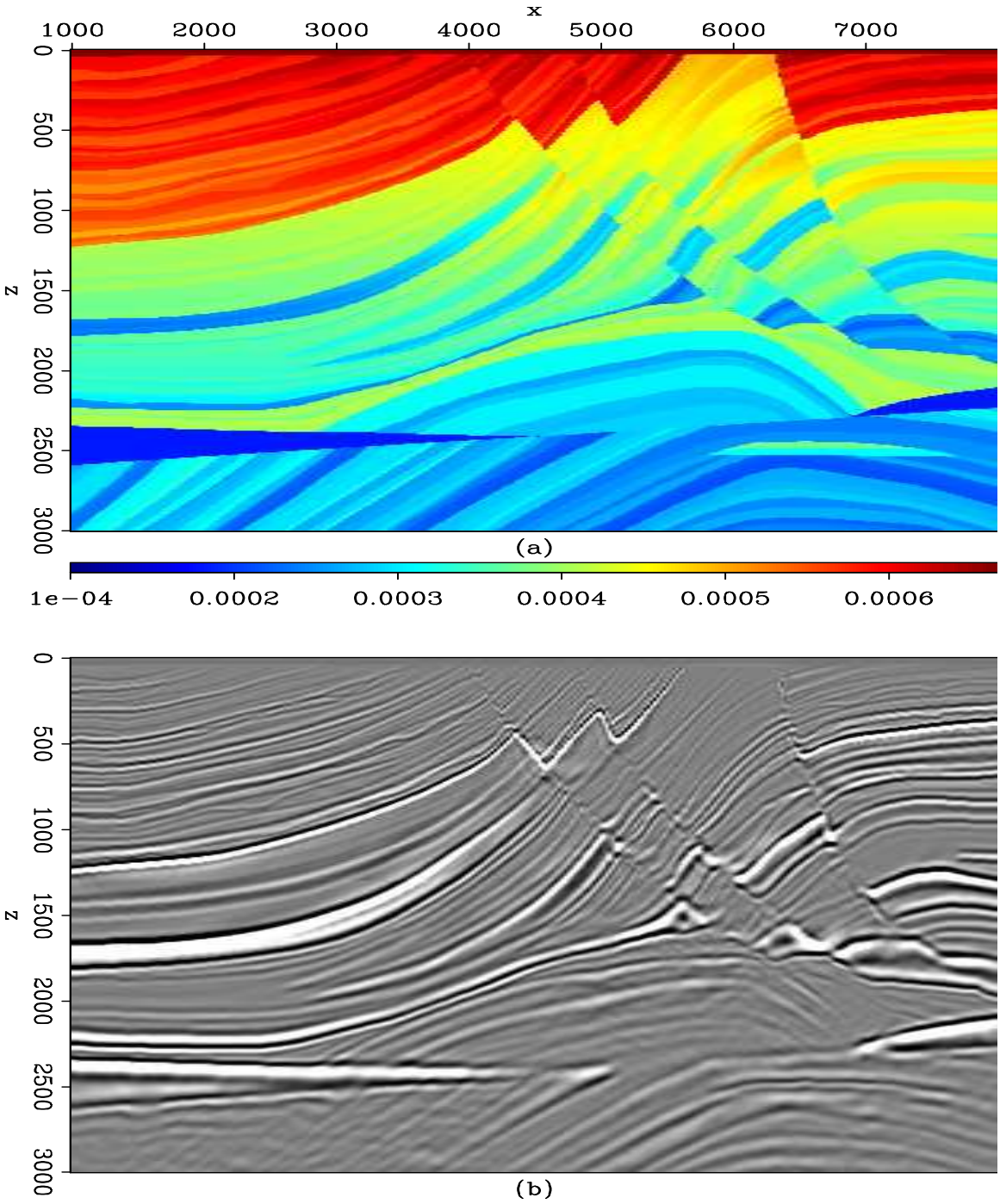

Figure 1:]

(a) True slowness of the Marmousi model. (b) Zero-subsurface offset section of the one-way shot-profile migration with the true slowness model.[**CR**]

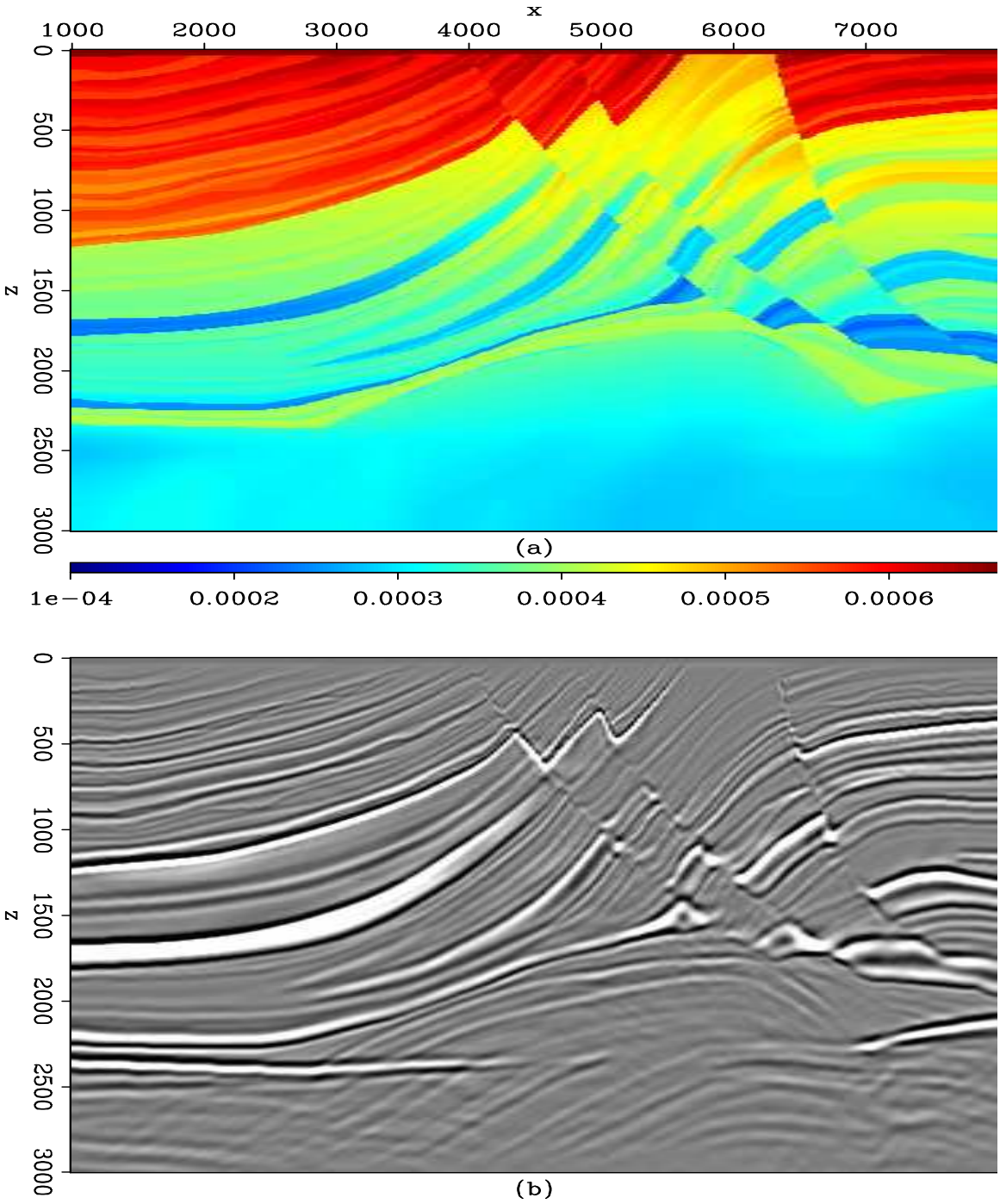

Figure 2:]

(a) Background slowness. (b) Zero-subsurface offset section of the one-way shot-profile migration with the background slowness model.[**CR**]

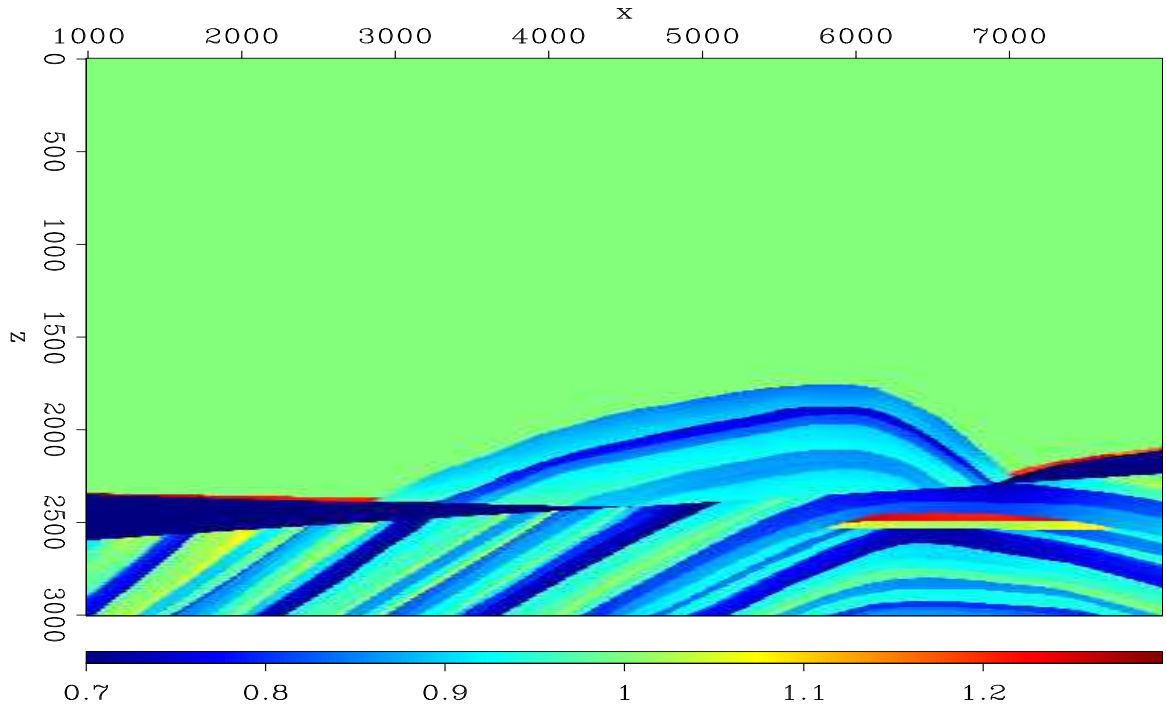

Figure 3:]

Slowness ratio.[**ER**]

Guerra –

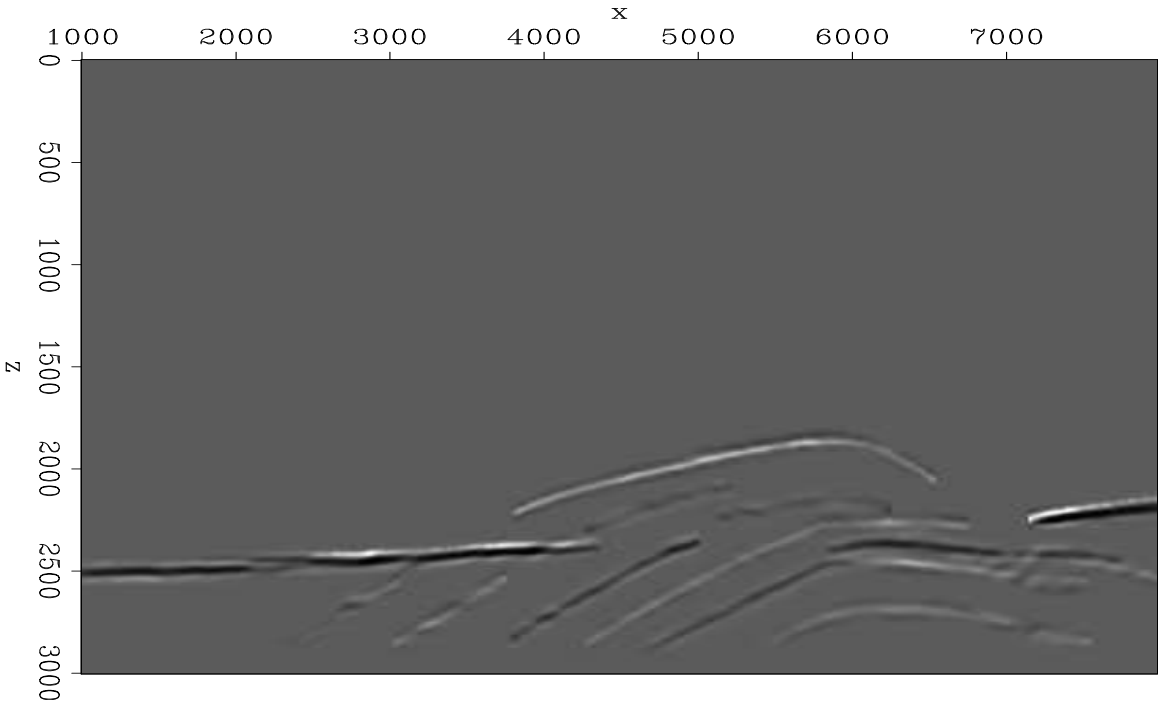

Figure 4:]

Zero-subsurface offset section showing the reflectors selected on the one-way shot-profile migration with the background slowness model.[**CR**]

Guerra –

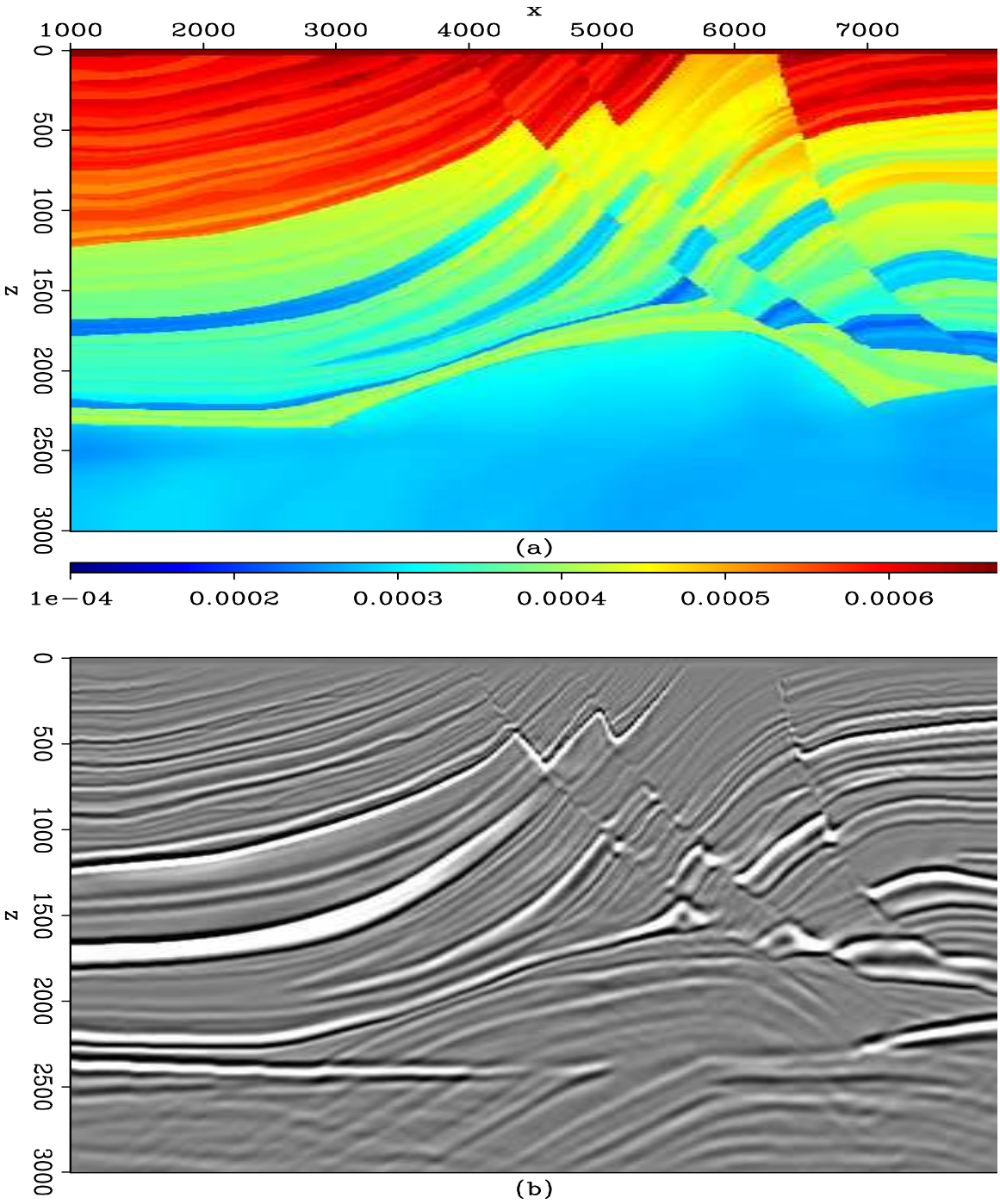

Figure 5:]

(a) Optimized slowness after 4 iterations with 41 function and gradient evaluations. (b) Zero-subsurface offset section of the one-way shot-profile migration with the optimized slowness model.[**CR**]

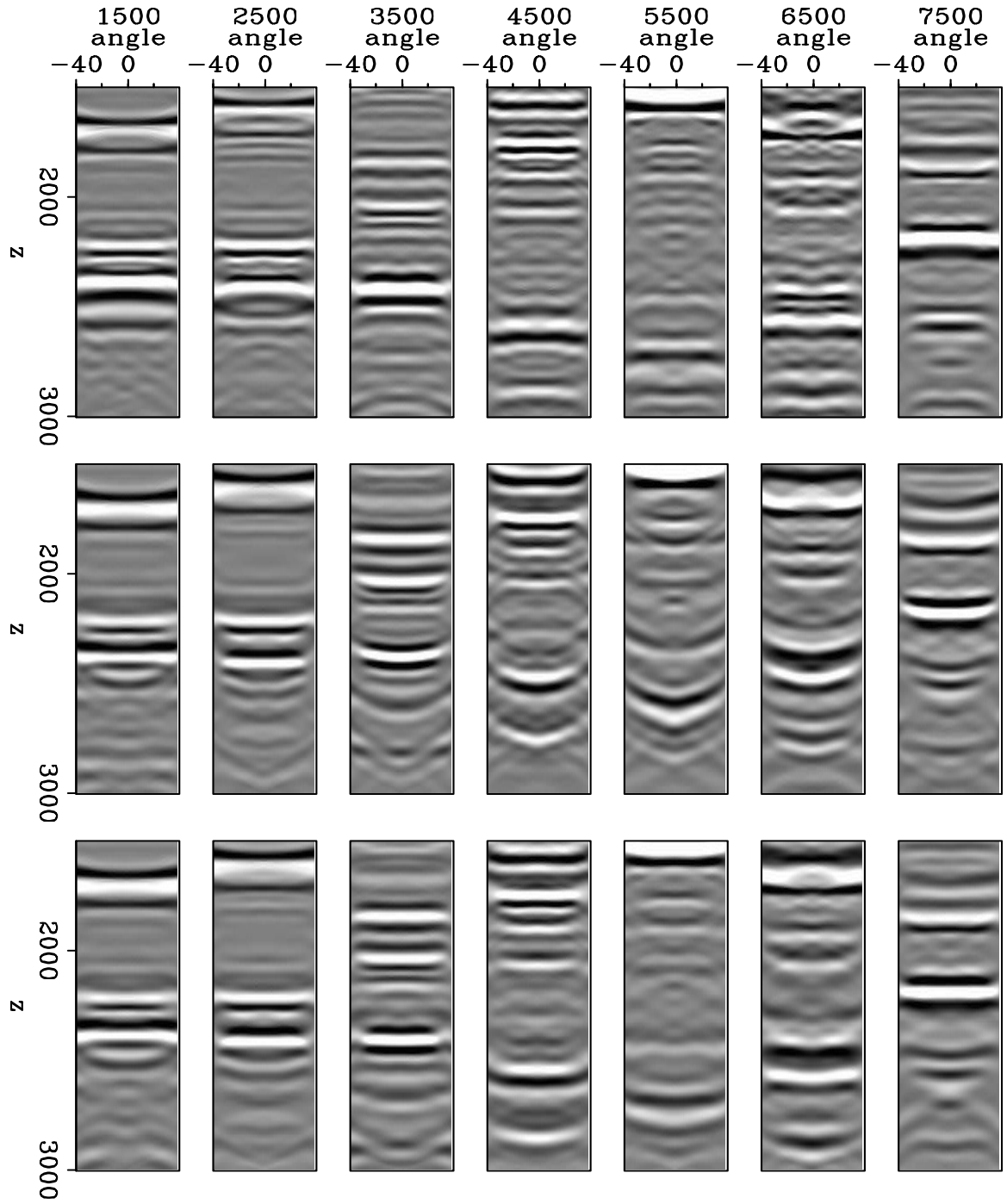

Figure 6:]

ADCIGs obtained with true slowness (top), background slowness (center), and optimized slowness (bottom).[**CR**]